

A STUDY OF THE FRACTURE BEHAVIOR OF DEFECTIVE  
WELDED STEEL CONNECTIONS DURING EARTHQUAKE

Tetsuro ONO (I)  
Shin-ichiro NAKAGAWA (II)  
Presenting Author: S.NAKAGAWA

SUMMARY

The purpose of this paper is to determine the critical value of fracture of defective structural members after crack propagation and thereby to measure quantitatively the fracture deformability of beam-column connections under strong ground motion. The results of experiments on defective connections are compared with those on notched plate specimens to obtain a relational expression of defect length, deflection amplitude, and number of cycles to fracture based on the COD concept in non-linear fracture mechanics.

1. INTRODUCTION

With the increase in size and complexity of structure, higher performance is increasingly demanded of steel members. Beam-column connections of a rigid frame are subjected to greater stress than any other members of the frame during earthquake. Thus, in order to ensure the safety of structures, it is essential to measure the deformation capacity of beam-column connections. It has been pointed out that defective welded connections are likely to break much earlier than sound welded connections assuming the same amount of frame deformation. In this light, it is necessary to study the fracture deformability of connections employing fracture mechanical techniques instead of the conventional techniques based on strength of materials.

When steel members fracture, causing considerable plastic deformation, the COD (Crack (Tip) Opening Displacement) criterion proposed by Wells and Cottrell and the  $J_{IC}$  criterion devised by Begley and Landes based on Rice's finding that the J-integral value is path-independent are considered applicable. Even when defects cause stable fibrous crack propagation prior to fracture, the COD concept is largely applicable. Hence it is considered valid as a criterion for crack propagation against cyclic force during an earthquake. In view of the above-mentioned, defective beam-column connections under seismic load were subjected to a very low cycle fatigue test to evaluate the plastic deformation capacity of the connections based on the COD criterion.

2. SETTING THE CRITICAL COD VALUE USING NOTCHED PLATE SPECIMENS

In order to evaluate the deformation capacity of defective structural members which fracture after crack propagation in accordance with the COD criterion, the COD and the average strain (gauge length = 160 mm) were measured, respectively using notched plate specimens as shown in Fig. 1.

---

(I) Dr. Eng. Associate Professor of Nagoya Institute of Technology, JAPAN

(II) Graduate Student of Nagoya Institute of Technology, JAPAN

The gauge length used for the present experiment<sup>1,2</sup> was more than ten times the notch length, and the average strain can be assumed as a global strain (overall strain :  $\epsilon_\infty$ ) virtually free from the effect of notches.

Fig. 2 shows an idealized COD- $\epsilon_\infty$  relationship of notched plate specimen under uniaxial tension stress. COD- $\epsilon_\infty$  relationship is composed of four parts,<sup>3</sup> 1) small scale yielding condition, 2) net section yielding condition, 3) instability region due to the unstable extension process of plastic deformation, 4) gross section yielding condition. Fig. 3 shows an example of COD- $\epsilon_\infty$  curve. The COD- $\epsilon_\infty$  relationship becomes almost linear after the specimens turn fully plastic. However, as the crack propagates, the increment of COD increases until the linear relationship disappears. The value of COD at this point is assumed as the critical value of crack propagation  $\delta_c$ . From Fig. 4, it can be seen that the  $\delta_c$  value for a particular type of steel is almost constant (0.75 mm for SS-41, 0.60 mm for HT-60, and 0.45 mm for HT-80) regardless of the shape and size of specimens, except thin specimens of mild steel which are especially influenced by the local deformation in thickness direction. Therefore it is thought that  $\delta_c$  is an effective critical value for fracture behavior of steel members.

### 3. CYCLIC BENDING TEST ON DEFECTIVE BEAM-COLUMN CONNECTIONS

This section describes the very low cycle bending test conducted on defective beam-column connections. The specimens were of the shape and dimensions as shown in Fig. 5(a). SS-41 rolled H shape was used as the beam, to the end of which an end plate was butt welded. The end plate was jointed to the column with a high tensile strength bolt, to form a cantilever. For the purpose of the present test, three types of specimens were prepared: defect-free specimens (X-series), specimens having metal touch type defects in the welded joint to the end plate (Y-series), and specimens having defects and subjected to welding with backing strip (Z-series). Details of the specimens are shown in Fig. 5(b).

Fig. 6(a), (b), (c) show the loading system and the gauge locations. The load is detected by a load cell installed to the head of a hydraulic jack. Displacement transducers and clip gauges are provided to measure the deflection of beam tip of specimens and the COD of defects, respectively. Values obtained by the clip gauges were converted into values at the initial defect tip by using equations (1) and (2) based on BCS model<sup>4</sup> in fully plastic condition, irrespective of the crack propagation from defects.

$$\text{COD} = \frac{V(a)}{V(x)} \times V_{cl}. \quad \text{--- (1)}$$

$$V(x) = \frac{4W\sigma_y}{\pi^2 E} \int_{\chi}^{\pi/2} \ln \left| \frac{\sin(\chi+\phi)}{\sin(\chi-\phi)} \right| d\chi \quad \text{--- (2)}$$

$V_{cl}$ : Clip gauge displacement at distance  $x$  from defect edge.

$V(x)$ : COD at distance  $x$  from defect edge, obtained by equation (2).

$V(a)$ : COD at defect tip, obtained by assuming  $x = a$  in equation (2).

$\sigma_y$ : Yield stress.  
 $a$ : Half length of defect.  
 $W$ : Specimen width.  
 $x$ : Distance from defect edge.  
 $\chi$ :  $\pi x/W$ .  
 $\phi$ :  $\pi a/W$ .

The test was conducted at constant deflection amplitude in completely reversed bending condition. It was repeated until a crack from defects propagated through the beam flange. The designed defect length and deflection amplitude of individual specimens are shown in Table 1. Mechanical properties of materials and welding conditions are shown in Tables 2 and 3.

#### 4. INTERRELATIONSHIP OF LOAD, DEFLECTION AND COD OF SPECIMENS

Fig. 7 shows the relationship between load  $P$  and beam tip deflection  $\Delta$  under monotonic loading. It can be seen that the deformation capacity of specimens varies significantly according to the presence or absence of defects, and that the deformation capacity deteriorates as the defect length increases. Fig. 8 shows a COD- $\Delta$  curve. The COD- $\Delta$  relationship is almost linear after beam full plastic moment  $M_p$  is reached. However, due to crack propagation from the defect tip, the increment of COD against  $\Delta$  begins to increase when COD approaches 0.75 mm, and thereafter, COD sharply increases, causing the breakdown of specimens. In regard to defect-free specimens, crack propagated to the butt welded flange in tension side after local buckling of compression beam flange. But, onset of crack propagation from defect was confirmed in a state of small deformation, in defective specimens.

Fig. 9 and 10 show an example of  $P$ - $\Delta$  curve of cyclic bending specimens. The  $P$ - $\Delta$  relationship in the initial phase is represented by a stable loop. The shorter the initial defect length and the smaller the controlled deflection amplitude, the greater becomes the number of times a stable loop occurs. Following the stable loop, crack propagation causes the load to decrease, resulting in the breakdown of specimens. The greater the deflection amplitude, the sharper becomes the decrease of load. Also, as the crack propagation length increases, an inflection point arising from crack opening/closing begins to appear at the compression side of the hysteresis loop. Fig. 11 and 12 show the relationship between COD and  $\Delta$ . It can be seen that with any of the specimens COD and  $\Delta$  increased with the increase of load in each cycle, but that the increase of COD due to crack propagation caused the stable loop to slide upward. This phenomenon is particularly conspicuous with specimens having greater deflection amplitude. Fig. 13 and 14 show the value of COD under maximum tensile load in each cycle. As shown, COD gradually increased with the increase in the number of cycles, and eventually, COD sharply increased as the crack propagation proceeded, causing the breakdown of specimens. This phenomenon occurred earlier with specimens having greater defect length and deflection amplitude. As this experiment was carried out under cyclic bending conditions, crack did not propagate uniformly in length, so crack propagation length was largest at the surface of beam flange. And inclination angle between crack surface and end plate surface was about 45 degrees.

## 5. NUMBER OF CYCLES TO FRACTURE OF DEFECTIVE BEAM-COLUMN CONNECTIONS

Here, based on the above-mentioned results of experiment on notched plate specimens and results of monotonic bending test on beam-column connections, COD = 0.75 mm is defined as the critical value  $\delta_c$  for specimens subjected to cyclic loading. Fig. 15 and 16 show maximum tensile load  $P_m$  in each cycle, together with the number of cycles  $N$ . The arrow indicates the number of cycles at which  $\delta_c$  is reached. It can be seen that this point almost corresponds to the point at which the load declines sharply.

Incidentally, since the measured defect lengths of specimens were different from the designed defect lengths, direct comparison between specimens could not be made. To make up for this, the relation between the number of cycles at which  $\delta_c$  is reached and the measured defect length was subjected to regression analysis (Fig. 17) to obtain the relation between the designed defect length ( $a = 4, 8, 12$  mm) at each deflection amplitude ( $\Delta = \pm 2.0, \pm 2.5, \pm 3.0$  cm) and the number of cycles at which specimens fractured. Fig. 18 shows the relation between the number of cycles to fracture  $N_f$ , obtained by the above-mentioned method, and the controlled deflection amplitude  $\xi (= \Delta / \Delta_p)$  non-dimensionalized by deflection  $\Delta_p$  at the beam full plastic moment, on a logarithmic scale. From this figure, it can be seen that the values of  $N_f$  and  $\xi$  of specimens at defect lengths 4, 8, 12 mm are distributed almost linearly. Using regression analysis, those values can be expressed as follows:

$$\xi (N_f)^{0.156} = 2.63 \quad (a = 4.0 \text{ mm}) \quad \text{---} \quad (3)$$

$$\xi (N_f)^{0.137} = 2.41 \quad (a = 8.0 \text{ mm}) \quad \text{---} \quad (4)$$

$$\xi (N_f)^{0.134} = 2.22 \quad (a = 12.0 \text{ mm}) \quad \text{---} \quad (5)$$

Concerning the Z-series specimens (welded connections with backing strip), the presence of backing strip tends to alleviate the fracture behavior against defects, and the number of cycles to fracture is greater than that of Y-series specimens having the same defect length. On the other hand, welded connections with backing strip are sensitive to the change in defect length. Namely, as the defect length increases, the number of cycles to fracture decreases drastically.

## 6. CONCLUSIONS

In this paper, the deformation capacity of defective welded connections has been discussed based on the results of various tests. The conclusions obtained from the study are summarized below.

A tension test was conducted on notched plate specimens to obtain the critical COD, which was established for each steel type. The results of a cyclic bending test conducted on defective beam-column connections revealed that the deformation capacity of connections widely varies according to the presence or absence of defects and that the deformation capacity deteriorates as the defect length increases. Also, the fracture behavior of connections was studied using the value of  $\delta_c$  based on COD concept. The interrelationship of  $\delta_c$ , the number of cycles to fracture  $N_f$ , and non-dimensional deflection amplitude  $\xi$  could be quantitatively measured by regression analysis.

## 7. ACKNOWLEDGEMENTS

In writing this paper the authors are grateful to Sumitomo Metal Industries, Ltd. (Mr. M. KATO) and Tomoe-gumi Iron Works Ltd. (Mr. I. KUBODERA) for providing the test specimens.

## 8. REFERENCES

1. T. ONO and S. NAKAGAWA, "Fracture Behaviors of Notched Steel Plate Considering The Effects of Mechanical Properties and Welding Conditions", Proc. Annual Meeting Arch. Inst. Japan, 1759, 1982
2. T. ONO and S. NAKAGAWA, "The Effects of Plate Thickness on Fracture Behaviors of Notched Steel Plate", Proc. Annual Meeting Arch. Inst. Japan, 1463, 1983
3. M. TOYODA, et al., "Deformability in General Yielding Unstable Fracture of Weldments of Structure Steels", Journal of J. W. S., Vol. 145, 1979
4. B. A. BILBY, et al., "The Spread of Plastic Yielding from Notch", Proc. Roy. Soc. London, 1963

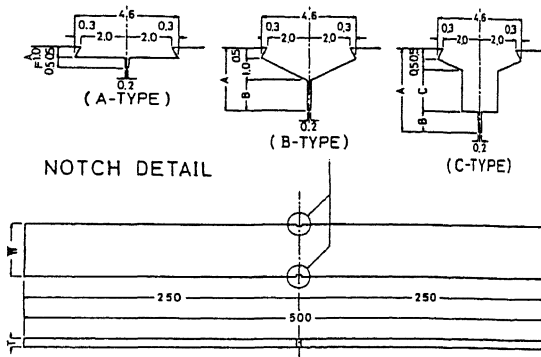


Fig. 1 Notched Plate Specimen (Unit:mm)

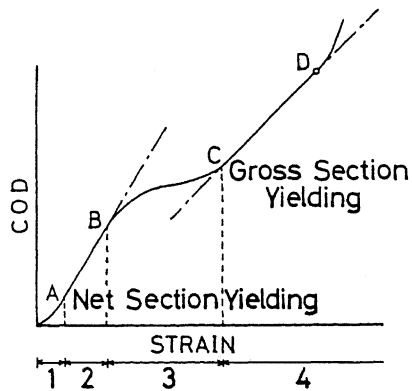


Fig. 2 Idealized COD- $\epsilon_{\infty}$  Curve

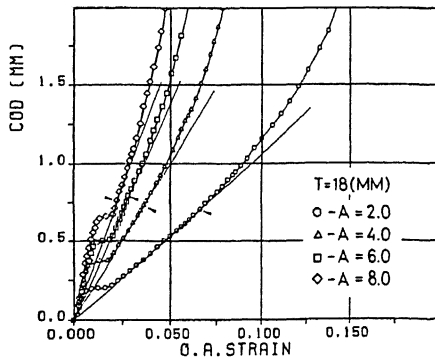


Fig. 3 COD- $\epsilon_{\infty}$  Curve

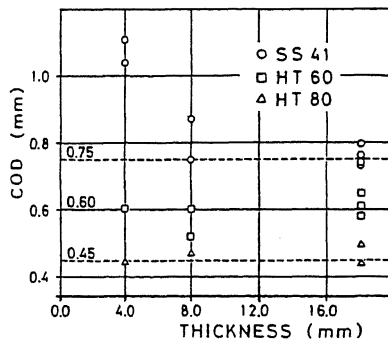


Fig. 4 Critical COD of Each Steel

Table 1 Specimen Dimensions

Specimen No.	A (mm)	Δ (cm)
I-H	0.0	Monotonic
I-3.0	0.0	±3.0
Y-L-H	4.0	Monotonic
Y-L-2.0	4.0	±2.0
Y-L-2.5	4.0	±2.5
Y-L-3.0	4.0	±3.0
Y-B-H	8.0	Monotonic
Y-B-2.0	8.0	±2.0
Y-B-2.5	8.0	±2.5
Y-B-3.0	8.0	±3.0
Y-12-H	12.0	Monotonic
Y-12-2.0	12.0	±2.0
Y-12-2.5	12.0	±2.5
Y-12-3.0	12.0	±3.0
Z-L-2.5	4.0	±2.5
Z-B-2.5	8.0	±2.5
Z-12-2.5	12.0	±2.5

Table 2 Mechanical Properties

	$\sigma_y$ (kg/mm <sup>2</sup> )	$\sigma_u$ (kg/mm <sup>2</sup> )	$\epsilon_y$ (×10 <sup>-4</sup> )	E (×10 <sup>4</sup> kg/mm <sup>2</sup> )	Elong. (%)
Flange	32.5	47.0	1550	2.11	21.0
Web	36.3	48.8	1730	2.10	23.6
Weld Metal	34.0	45.1	1620	2.10	30.5

Table 3 Welding Conditions

Series	Welding Rod (Diameter(mm))	No. of Passes	Welding Current (A)
X-Series	G200 (4φ)	2-3 (Surface)	160
		2 (Reverse)	160
Y-Series	G200 (4φ)	2-3 (Surface)	160
		2-3 (Reverse)	160
Z-Series	G200 (4φ)	6-9 (Surface)	160

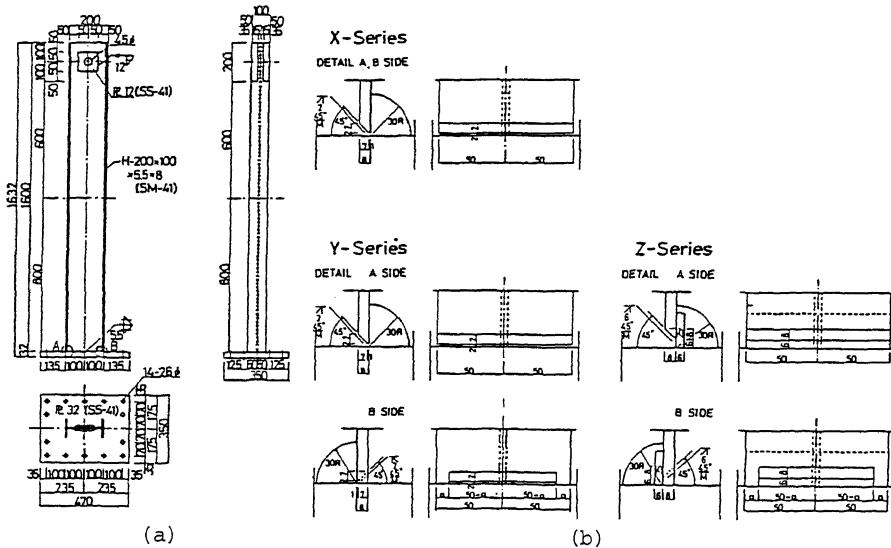


Fig. 5 Test Specimens (Unit:mm)

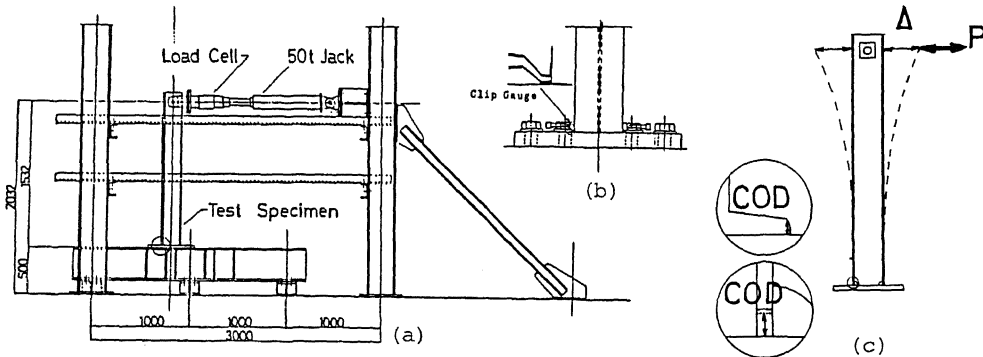


Fig. 6 Loading System and Gauge Locations (Unit:mm)

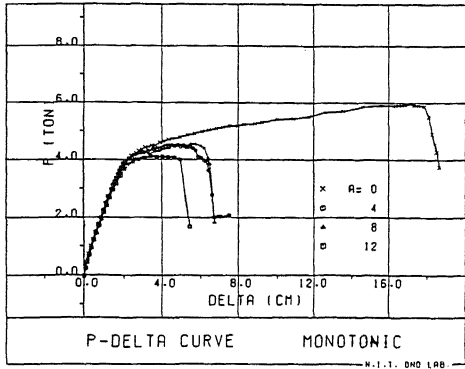


Fig. 7 P- $\Delta$  Curves  
under Monotonic Loading

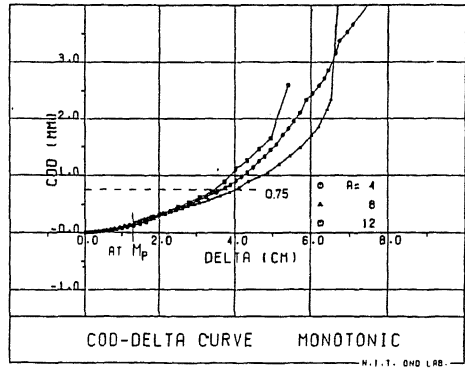


Fig. 8 COD- $\Delta$  Curves  
under Monotonic Loading

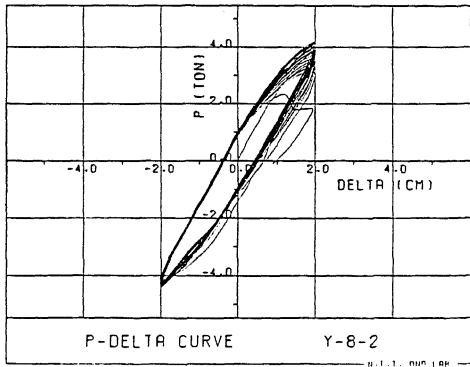


Fig. 9 Hysteresis Loops

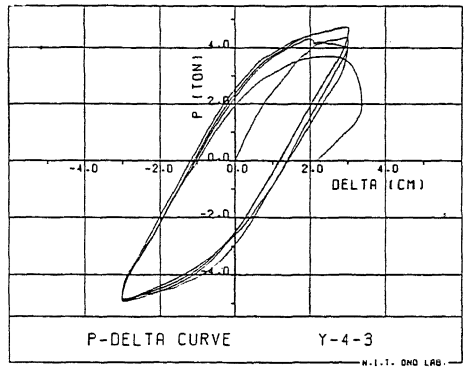


Fig. 10 Hysteresis Loops

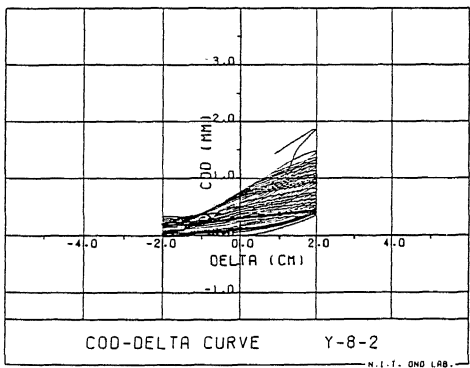


Fig. 11 COD- $\Delta$  Curves  
under Cyclic Loading

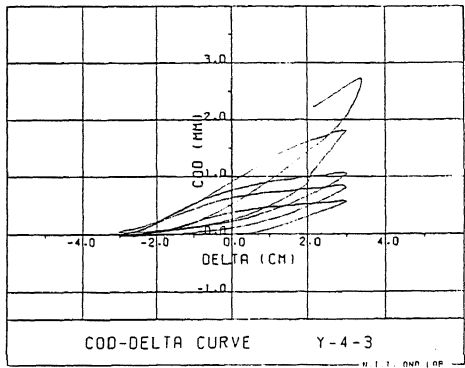


Fig. 12 COD- $\Delta$  Curves  
under Cyclic Loading

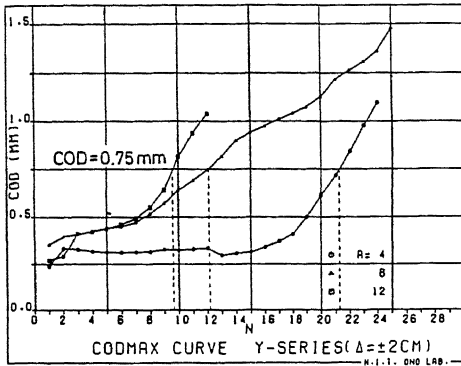


Fig. 13 COD at  $P_m$  in Each Cycle

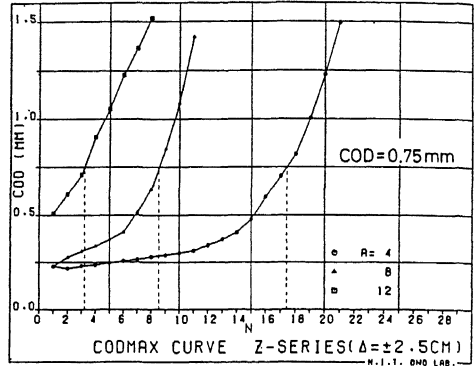


Fig. 14 COD at  $P_m$  in Each Cycle

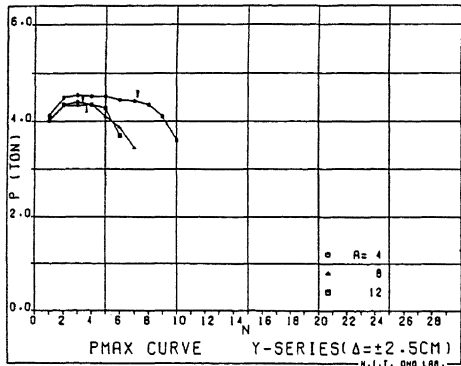


Fig. 15  $P_m$  in Each Cycle

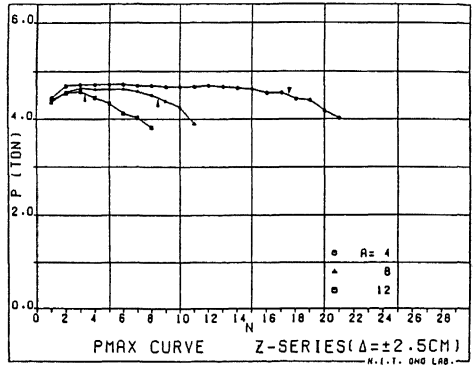


Fig. 16  $P_m$  in Each Cycle

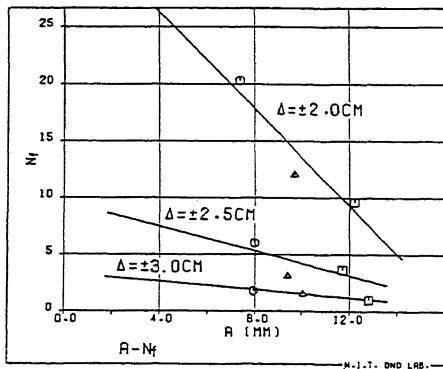


Fig. 17 Regression Analysis

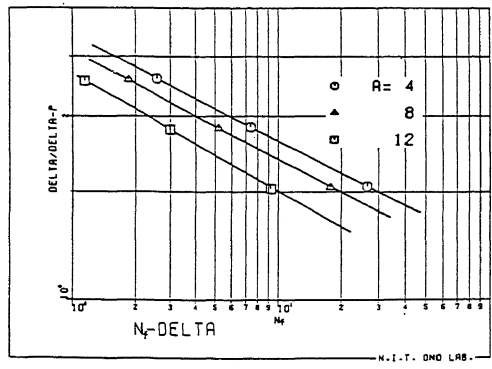


Fig. 18  $\xi$ - $N_f$  Relationships